Applied Catalysis B: Environmental 89 (2009) 41–48

Contents lists available at ScienceDirect

Applied Catalysis B: Environmental

journal homepage: www.elsevier.com/locate/apcatb

Structure and NO_x storage behaviour of flame-made $BaCO_3$ and $Pt/BaCO_3$ nanoparticles

M.O. Symalla [a,*], A. Drochner [a], H. Vogel [a], R. Büchel [b,c], S.E. Pratsinis [b], A. Baiker [c]

[a] Technische Universität Darmstadt, Ernst-Berl-Institut für Technische und Makromolekulare Chemie, Petersenstr. 20, D-64287 Darmstadt, Germany
[b] ETH Zürich, Department of Mechanical and Process Engineering, Sonneggstrasse 3, CH-8092 Zürich, Switzerland
[c] ETH Zürich, Department of Chemistry and Applied Biosciences, Hönggerberg, CH-8093 Zürich, Switzerland

ARTICLE INFO

Article history:
Received 13 August 2008
Received in revised form 12 November 2008
Accepted 14 November 2008
Available online 24 November 2008

Keywords:
Lean NO_x trap
NO_x storage
Flame spray pyrolysis
Nanoparticles
$BaCO_3$
$Pt/BaCO_3$
Platinum
BaO
In situ
DRIFTS
NO_2
NO breakthrough curve
Barium nitrate
Barium nitrite

ABSTRACT

$BaCO_3$ and $Pt/BaCO_3$ nanoparticles with high specific surface area (SSA) were prepared by flame spray pyrolysis (FSP). Their structure and behaviour during NO_x storage were investigated with special focus on the mechanistic and kinetic details. NO exposure of $BaCO_3$ (BET: 45 $m^2 g^{-1}$) at various temperatures resulted in simple NO adducts. Low NO storage rate and NO_x storage capacity (NSC) were observed up to 400 °C. In the presence as well as the absence of oxygen, NO was stored on $BaCO_3$ showing the same IR-adsorption bands at 100–300 °C. Higher NSC and storage rates were observed for NO_2 adsorption. DRIFT spectra showed that NO_2 adsorption is accompanied by the formation of small amounts of NO which could be stored and subsequently oxidised again to NO_2 adducts.

$Pt/BaCO_3$ prepared under identical conditions resulted in higher SSA (110 $m^2 g^{-1}$) and showed increased NSC especially at higher temperatures. Enhanced DRIFT adsorption bands indicated the same NO adducts as obtained for the Pt-free $BaCO_3$ during NO treatment. In the presence of oxygen and above the light-off temperature for NO oxidation, the consecutive reaction of stored nitrite to nitrate could be observed by in situ DRIFTS. NO_2 adsorption led again to the highest NSC and storage rate. An optimal operation temperature window around 300 °C was found where the NO_2 storage rate was high and the catalysed competing NO_2 conversion to NO was low enough to afford maximal NSC. Structural investigations indicate that only prolonged NO_x treatment leads to bulk barium nitrate: solid state conversion occurs after few hours. This supports the contention that the main contribution to NO_x storage during technical application in NSR catalysis occurs in the surface and subsurface regions of $BaCO_3$.

1. Introduction

Global climate change is mainly caused by the increasing emission of carbon dioxide and other greenhouse gases. Finally, extreme CO_2 emissions lead to drastic ecological, health and economic damages. Thus the reduction of all greenhouse gases is perhaps the largest looming public challenge we face today [1,2]. Legislative regulations can force e.g. the automotive industry to produce vehicles with low CO_2 emissions. In this context diesel and lean burn engines are becoming more important. These engines possess intrinsic challenges with NO_x after-treatment in lean atmosphere. Beside selective catalytic reduction (SCR), another promising solution for passenger cars is the so-called NO_x storage reduction (NSR) catalyst or "Lean NO_x trap" (LNT) [3,4]. NO_x is stored under fuel lean conditions and is reduced during short fuel rich periods to harmless nitrogen. NSR catalysts consist of more than one component. Typically an alumina support carries ceria for oxygen and low temperature NO_x storage [5]. Additionally alkali metal oxides and alkaline earth metal oxides, especially BaO are needed for high temperature NO_x storage. Noble metals like Pt are used for the NO oxidation [6] during lean phases and for NO_x reduction during rich phases.

Several papers account for NO_x storage on BaO [7–9] or BaO-containing systems [10–13], but only some consider the presence of CO_2 in the exhaust gas that reacts with BaO to $BaCO_3$ [14–20]. The carbonate changes NO_x storage properties reducing the NO_x storage capacity (NSC). Studies of NO_x adsorption on Pt/Ba/alumina catalysts in which the barium component consists mainly of barium carbonate [15,21,22] show that NO_x reacting with surface barium sites forms barium nitrate which is much less thermally stable than bulk barium nitrate. These results emphasise the dependency of the storage behaviour on Ba loading and interfacial contact to the support. Nevertheless, to understand technical NSR catalysts and their storage behaviour under real working conditions in detail, it is

* Corresponding author. Tel.: +49 6151 16 2065; fax: +49 6151 16 3465.
E-mail address: symalla@ct.chemie.tu-darmstadt.de (M.O. Symalla).

0926-3373/$ – see front matter © 2008 Elsevier B.V. All rights reserved.
doi:10.1016/j.apcatb.2008.11.020

also beneficial to elucidate NO_x and particularly NO adsorption on pure $BaCO_3$ and Pt-loaded $BaCO_3$. A powerful technique to detect NO_x adsorbates in situ is diffuse reflectance infrared Fourier transform spectroscopy (DRIFTS). The low surface areas of commercially available $BaCO_3$ and resulting small intensities of the adsorption bands limit detection and interpretation of the DRIFTS spectra. For this reason, high SSA $BaCO_3$ and $Pt/BaCO_3$ were made by flame spray pyrolysis [23]. These nanopowders served as model systems for studying NO_2 as well as NO adsorption on $BaCO_3$, the major storage component in NSR catalysts under real conditions.

2. Experimental

2.1. Commercial samples and preparation of high SSA powders

Commercially available BaO (Acros organics, 95% extra pure, granulate) and $BaCO_3$ (Acros organics, 99.999%, extra pure) were compared with flame-made $BaCO_3$ and $Pt/BaCO_3$. These materials were prepared using liquid barium 2-ethylhexanoate (30% in xylene, STREM chemicals) mixed in a 1:1 volume ratio with 2-ethylhexanoic acid (Riedel-de Haën, purum). For $Pt/BaCO_3$ additionally platinum(II) acetylacetonate (STREM, 98%) was added in order to get a Ba to Pt weight ratio of 20:1. The liquid precursor was then fed at 3 mL min^{-1} into the flame spray pyrolysis (FSP) reactor as described earlier [24] and dispersed with 8 L min^{-1} O_2 (PanGas, technical grade). The as-formed spray was ignited through a premixed pilot flame O_2/CH_4 (PanGas, purity 2.5) in the ratio of 2:1.

2.2. Sample characterisation and transient NO_x storage tests

IR spectra on powders were recorded in situ via DRIFTS. A FT-IR spectrometer (Bio-Rad, FTS 175 C) with a heatable reactor chamber [25], a 3D-praying mantis mirror system (Harrick) and a MCT detector were used. The resolution of the recorded spectra is 4 cm^{-1}. The catalyst powder was deposited in a quartz frit and placed in the reactor chamber. Gaseous components were fed into the reaction chamber and subsequently through the catalyst powder.

To obtain NSC values, NO_x breakthrough curves were measured using a quartz glass tubular reactor, surrounded with a heatable aluminium block. The gas outlet was analysed with a chemiluminescence detector (CLD–EcoPhysics 700 el ht).

The reaction gas mixtures for NO measurements consisted of 1000 (for DRIFTS experiments) or 100 (for NSC experiments) vol. ppm NO (Linde—2.5 vol.% NO purity 2.5 in Ar purity 5.0) balanced with nitrogen (Messer—purity 5.0) and optional with 10 vol.% oxygen (Messer—purity 3.5). NO_2 adsorption experiments were performed with NO_2 (Messer—1.51 vol.% NO_2 purity 1.8, stabilised with 5.28 vol.% O_2 purity 4.5) balanced with nitrogen to obtain the same concentrations as mentioned above. The gases were fed by mass flow controllers (Bronkhorst and Brooks) with a total flow rate of 140 mL min^{-1} (SV = 16 000 h^{-1}).

Prior to the adsorption experiments, the samples were pretreated with 30 vol.% oxygen (Westfalen—purity 3.5) in nitrogen at 300 °C for 1 h. The adsorption temperature was subsequently set under nitrogen atmosphere.

NO_x adsorption spectra were obtained by subtracting solid state spectra without NO_x from solid state spectra during NO_x treatment while the rest of the reaction conditions remained unchanged.

XRD patterns of the catalysts were measured on a STADI P (Stoe) diffractometer with a Cu-anode. The structure refinement according to the Rietveld method [26] was carried out with the software "FullProf" [27], integrated in the WinPLOTR software package.

For transmission electron microscopy (TEM) the powder samples were dispersed in ethanol and deposited onto a perforated carbon foil supported on a copper grid (Okenshoji Co. Ltd.) performed on a CM30 (FEI; LaB6) operated at 300 kV.

3. Results and discussion

3.1. Structural studies

3.1.1. Flame-made $BaCO_3$

Particles with SSA of 45 m^2 g^{-1} were produced here. Fig. 1 shows "bean-like" shaped particles about 25 nm wide and 25–100 nm long, that are similar but smaller than reported in the literature [28]. Fig. 2 shows that they were orthorhombic $BaCO_3$, 5 h after synthesis, meaning that only little or no monoclinic $BaCO_3$ was formed [28]. After calcination at 400 °C in air for 1 h the SSA decreased by less than 10% to about 41 m^2 g^{-1}.

3.1.2. Flame-made $Pt/BaCO_3$

The addition of Pt to $BaCO_3$ resulted in a markedly higher SSA of 110 m^2 g^{-1} which decreased to 60 m^2 g^{-1} after calcination. In Fig. 3a the TEM of fresh FSP-made $Pt/BaCO_3$ is shown. A fine, nanometre sized mesh-like structure of $Pt/BaCO_3$ is responsible for the high SSA. The Pt clusters decrease the surface energy of the

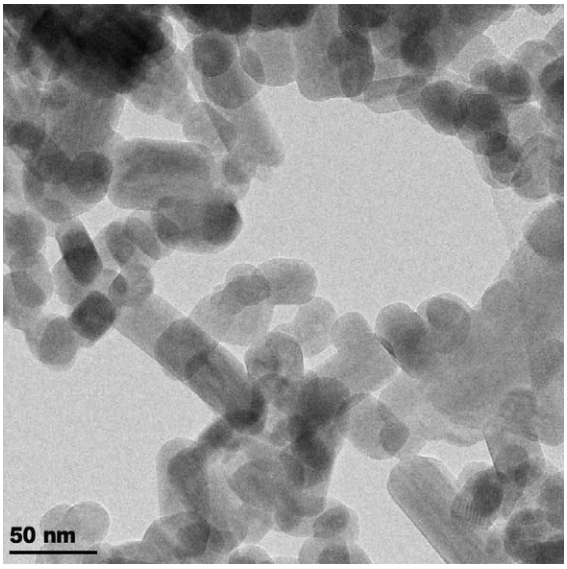

Fig. 1. TEM image of fresh flame-made $BaCO_3$.

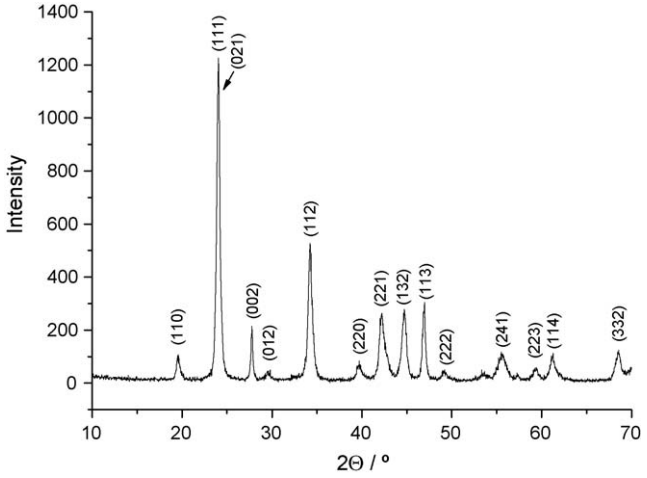

Fig. 2. XRD of the fresh flame-made $BaCO_3$.

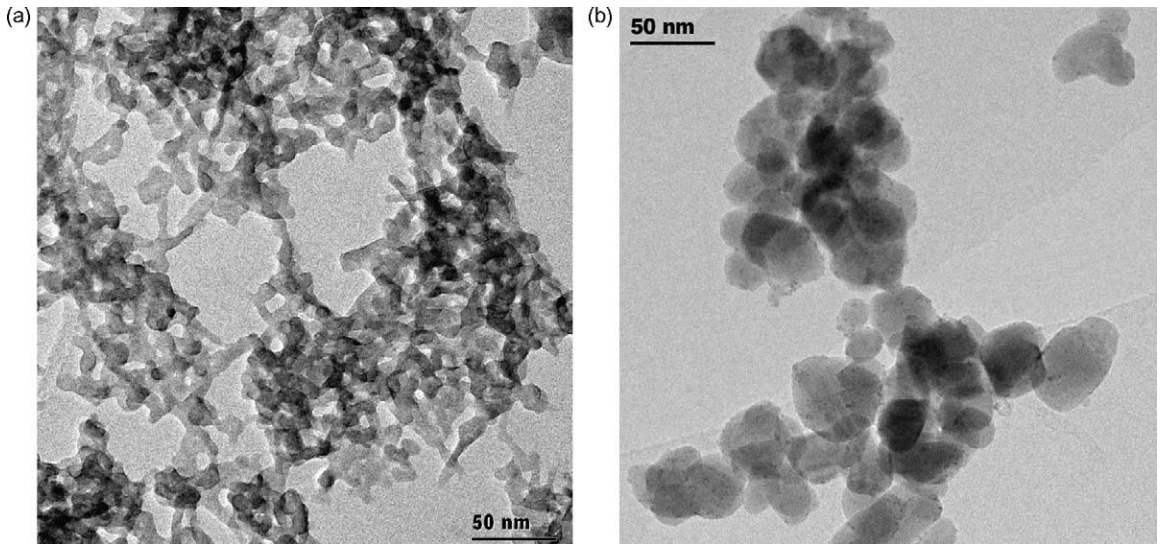

Fig. 3. TEM images (a) fresh $Pt/BaCO_3$ and (b) $Pt/BaCO_3$ pre-treated with N_2/O_2 at 400 °C.

$BaCO_3$ crystallites hindering its surface growth (Zener pinning) during the short residence time in the flame [29]. When sintered at elevated temperatures (400 °C, 1 h) these structures changed into a spheroid shape as seen in Fig. 3b which resembled the pure $BaCO_3$ from Fig. 1. Fig. 4a shows the XRD pattern of freshly prepared powder indicating the presence of monoclinic $BaCO_3$ [30] which was stable for several days, probably due to the presence of Pt. After calcination in air at 400 °C, a phase change to the more stable orthorhombic $BaCO_3$ [31] was observed (Fig. 4b).

3.2. NO_x adsorption on commercially available BaO and $BaCO_3$

Fig. 5a shows the DRIFT spectra of BaO after 30 min of NO_x treatment at 200 °C. Only a single band at 1246 cm^{-1} with low intensity arises during NO treatment. This indicates that the surface is probably mainly covered by one type of species. In the presence of oxygen (10 vol.%) during NO adsorption, the intensity of the band at 1246 cm^{-1} was increased while bands at 1376 and 1336 cm^{-1} became discernible that are assigned to nitrates from NO_2 adsorption on BaO. The strongest band at 1246 cm^{-1} which could be observed during NO adsorption was probably due to adsorbed NO. The NO formation may proceed via the well-discussed overall reaction [8,14,32,33]:

$$BaO + 3NO_2 \rightarrow Ba(NO_3)_2 + NO \quad (1)$$

All three bands show different formation kinetics during NO_2 treatment and belong consequently to different species. The overall storage rate as well as the intensity of the bands increases during adsorption at 300 °C (see Fig. 5b). In addition to these bands, new ones at 1775 and 1500 cm^{-1} were formed after 30 min NO_2 treatment. According to the solid state spectra of $Ba(NO_3)_2$ (cf. Fig. 11a), these bands can be assigned to solid state nitrate bands. That means NO_2 adsorption occurred beside the solid state conversion which is fast enough at 300 °C. NO_2 adsorption at 100 °C led only to adsorption bands with an intensity of 0.2 ($-\lg R$) after 30 min NO_2 treatment.

No bands were detectable during NO or NO/O_2 adsorption on commercial $BaCO_3$. Only NO_2 treatment showed small gas phase bands of dosed NO_2 at 1600 and 1630 cm^{-1} and formation of weak adsorption bands around 1350 cm^{-1} (see Fig. 5a). These adsorption bands are located in the same region as the nitrate bands during NO_2 adsorption on BaO. Thus NO_2 adsorption on $BaCO_3$ leads to the same species.

The NSC as well as the band intensities of NO_2 storage on $BaCO_3$ was much lower than on BaO which is, in this case, not attributable to the different SSA (BET_{BaO}: 0.2 $m^2\,g^{-1}$ and BET_{BaCO_3} : 1 $m^2\,g^{-1}$). That means that the more active component for NO_x storage is BaO but in catalysts under real working conditions the Ba component consists mainly of $BaCO_3$ [14]. To enable DRIFTS detection of adsorbates especially for NO treatment, $BaCO_3$ with higher BET surface was prepared by FSP.

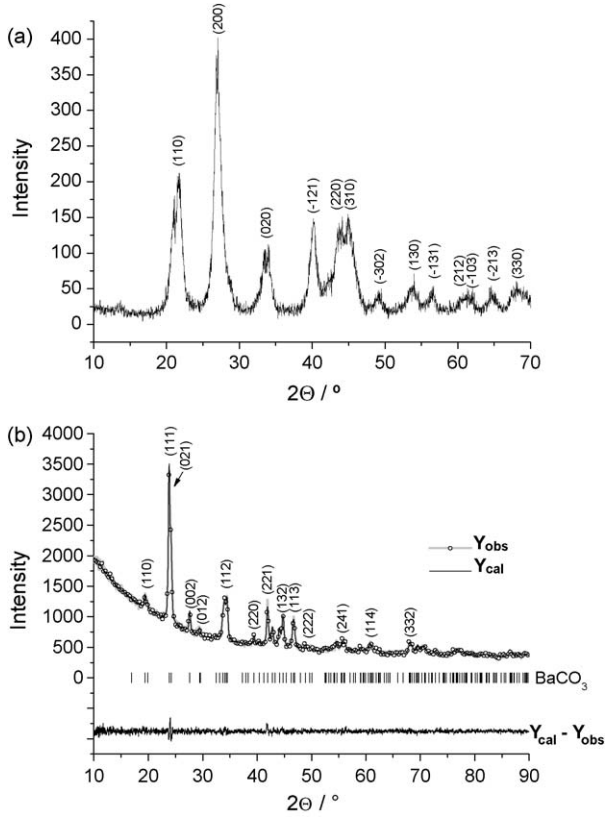

Fig. 4. XRD of (a) fresh $Pt/BaCO_3$ and (b) $Pt/BaCO_3$ pre-treated with N_2/O_2 at 400 °C.

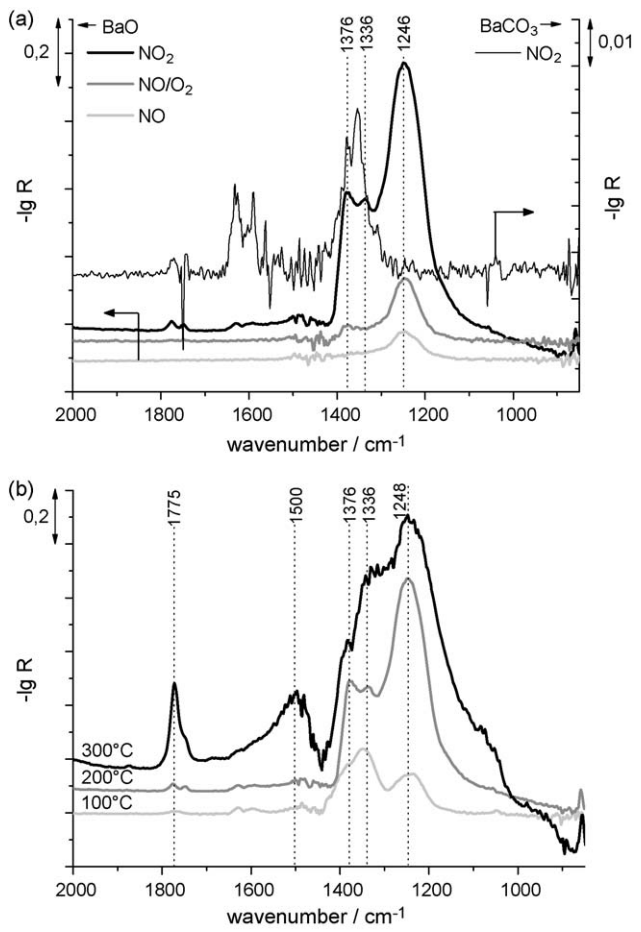

Fig. 5. (a) DRIFT spectra of NO, NO/O_2 and NO_2 adsorption on commercial BaO (left scale) and NO_2 adsorption on commercial $BaCO_3$ (right scale) at 200 °C after 30 min. (b) NO_2 adsorption on commercial BaO at 100, 200 and 300 °C.

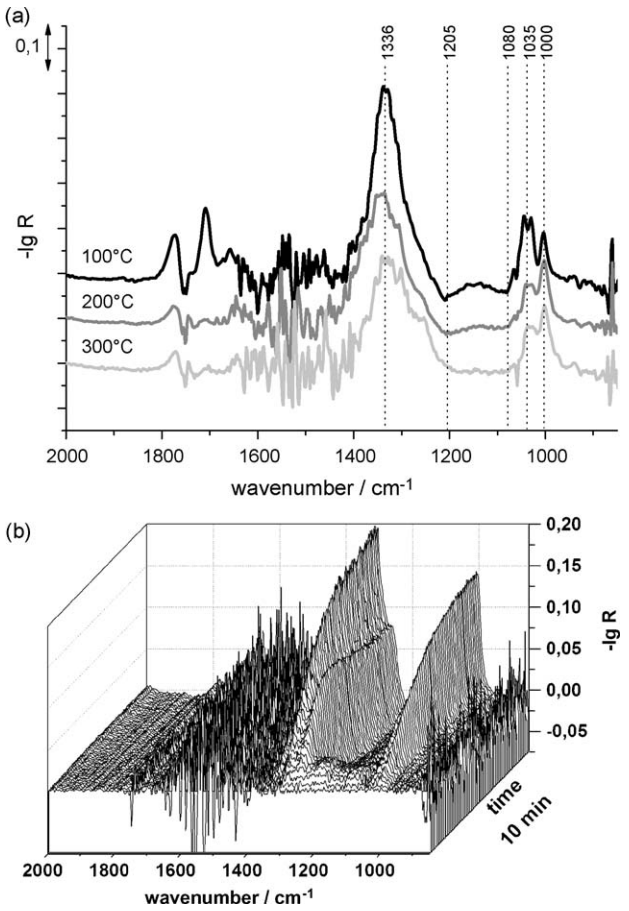

Fig. 7. (a) Temperature dependence of NO_2 storage on flame-made $BaCO_3$ after 30 min. (b) Development of DRIFT spectra during 10 min of NO_2 treatment of flame-made $BaCO_3$ at 200 °C.

3.3. NO_x adsorption on high SSA $BaCO_3$

High SSA $BaCO_3$ was prepared (untreated 45 $m^2\,g^{-1}$ and after calcination 41 $m^2\,g^{-1}$) and on this material NO_x adsorption led to detectable bands at 1300–1000 cm^{-1} (Fig. 6). After 30 min of NO exposure, bands appeared at 1205 and 1080 cm^{-1} with high intensities while the bands at 1035 and 1000 cm^{-1} remained small which is in contrast to the later shown NO_2 adsorption. As neither molecular oxygen in the gas phase nor oxide anions in the lattice (there are only CO_3^- anions) were present, the formed species and their bands are attributed to simple NO adducts. Different adsorption geometries are conceivable to explain the variety of the obtained bands. Temperature variation from 100 to 300 °C showed no change in these bands, except at 300 °C where their intensities decreased marginally. The presence of oxygen during NO adsorption on $BaCO_3$ led to formation of the same bands that increased only marginally with higher temperatures. A bordered region of noise was detected from 1650 to 1400 cm^{-1} and could only be observed in spectra of powder samples with high SSA. The origin of the noise remains unclear.

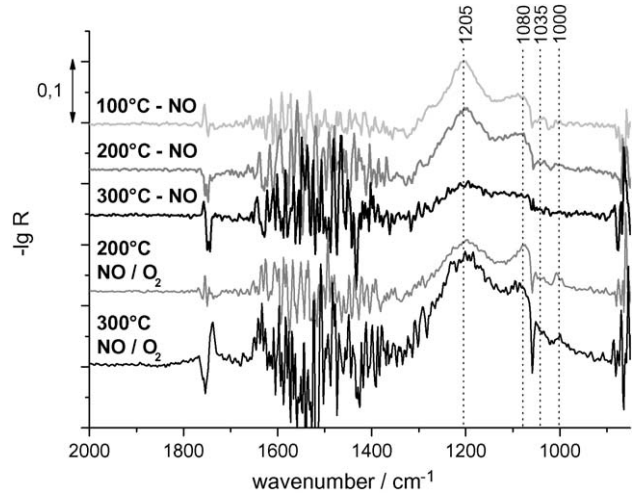

Fig. 6. NO_x storage on flame-made $BaCO_3$ at different temperatures after 30 min.

For NO_2 adsorption on $BaCO_3$ additional bands were obtained as seen in Fig. 7a. The strongest band is located at 1336 cm^{-1} attributed to nitrates as observed during NO_2 treatment on BaO. In this context Schmitz and Baird [8] discuss the nomenclature of adsorbed species on BaO and define (NO_2^-) as nitrite and (NO_3^-) as nitrate species. Most discussed nitrates were formed from adsorbed NO_2 on lattice oxide ions. If we assume that $BaCO_3$ only consists of barium cations as well as carbonate anions (CO_3^{2-}) (oxide anions, O^{2-}, should be absent) and NO_x adsorbed on carbonate sites, the discussion concerning nitrite and nitrate species would become difficult. To simplify, we assume the presence of oxide on the barium carbonate surface by decarbonation during NO_x treatment [14]. Then adsorbed NO_2 leads naturally to nitrate bands and NO adsorption on the surface results in nitrite formation. Furthermore the bands at 1035 and 1000 cm^{-1} were intensified during NO_2 treatment. Variation of the temperature at 100–300 °C led only to changes in the intensity of the obtained bands.

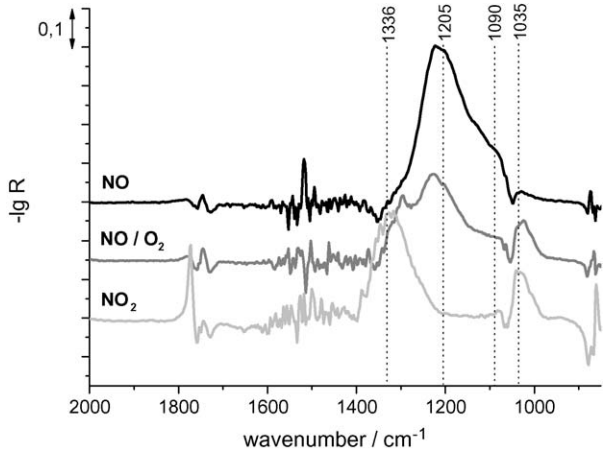

Fig. 8. Influence of gas composition during adsorption on $Pt/BaCO_3$ at 200 °C after 30 min.

Regarding the kinetics of the band at 1205 cm^{-1}, a maximum intensity could be observed initially during NO_2 adsorption. This is shown in Fig. 7b for NO_2 adsorption at 200 °C with the maximum intensity after 1 min. The band of the intermediate species represents the vibration mode of a nitrite as seen in Fig. 6. NO might be formed during NO_2 treatment according to Eq. (1) [14] and after its adsorption on $BaCO_3$, gaseous NO_2 oxidises it.

3.4. Influence of platinum: NO_x adsorption on $Pt/BaCO_3$

Adsorption measurements of NO, NO/O_2 and NO_2 were performed on $Pt/BaCO_3$ (Fig. 8). To single out the effect of Pt during NO_x storage, the same reaction conditions were applied noting, however, that the sample SSA was 110 $m^2\ g^{-1}$ before pre-treatment and 60 $m^2\ g^{-1}$ before NO_x adsorption. Adsorption of NO at 200 °C led qualitatively to the same nitrite bands as obtained during NO treatment on $BaCO_3$. Comparing these band intensities during NO adsorption, the intensities of the obtained bands during NO adsorption on $Pt/BaCO_3$ were significantly enhanced (Figs. 6 and 8). This was probably caused by the higher SSA of $Pt/BaCO_3$ than $BaCO_3$ (BET: 41 $m^2\ g^{-1}$). Note that the higher intensity of the observed nitrites and nitrates after exposure to NO somehow stands in contrast to similar studies performed on conventional Pt/Ba/alumina catalysts, where higher intensities are observed after exposure to NO_2 [13]. The reason for this behaviour is not clear yet but may be tentatively attributed to the different material ($BaCO_3$) and the fact that different adsorbed species might have altered extinction coefficients.

In the presence of oxygen at 200 °C the nitrite bands at 1205 and 1090 cm^{-1} exhibited a maximum after 5 min and new bands (1336 and 1035 cm^{-1}) were formed (the spectrum after 30 min NO/O_2 storage is shown in the middle of Fig. 8). These new bands were already observed during NO_2 adsorption on $BaCO_3$ and could be assigned to nitrate. This means that nitrite species were oxidised to nitrate during NO/O_2 storage. This oxidation was not observed during NO/O_2 storage on $BaCO_3$, and therefore the effect can be ascribed to Pt which is a well-known catalyst for NO oxidation. The onset of this reaction depends on the support, Pt dispersion [34] as well as the feed composition [6,35]. Typically NO oxidation starts at 100–200 °C. Thus it is reasonable to assume that formed NO_2 acts as oxidant and reacts with the adsorbed nitrites to nitrates. Additionally the direct storage of in situ formed NO_2 is possible.

The observed consecutive reaction showed strong temperature dependence (see Fig. 9a). NO/O_2 adsorption at 100 °C led to the same adsorption bands as NO adsorption without oxygen. Only the band intensities were increased in the presence of oxygen but the oxidation reaction was too slow or did not take place. At 200 °C the oxidation of stored NO was fast enough to be observed via DRIFTS. Fig. 9b shows the kinetics of the nitrite bands at 1205 cm^{-1} for different temperatures, with and without oxygen. Increasing the storage temperature to 300 °C led to a faster consecutive reaction. The spectrum after 30 min NO/O_2 treatment is similar to the spectrum resulting from NO_2 treatment of $Pt/BaCO_3$ or $BaCO_3$. They all show nitrate bands in the regions of 1336 and 1035 cm^{-1} and negligible nitrite bands.

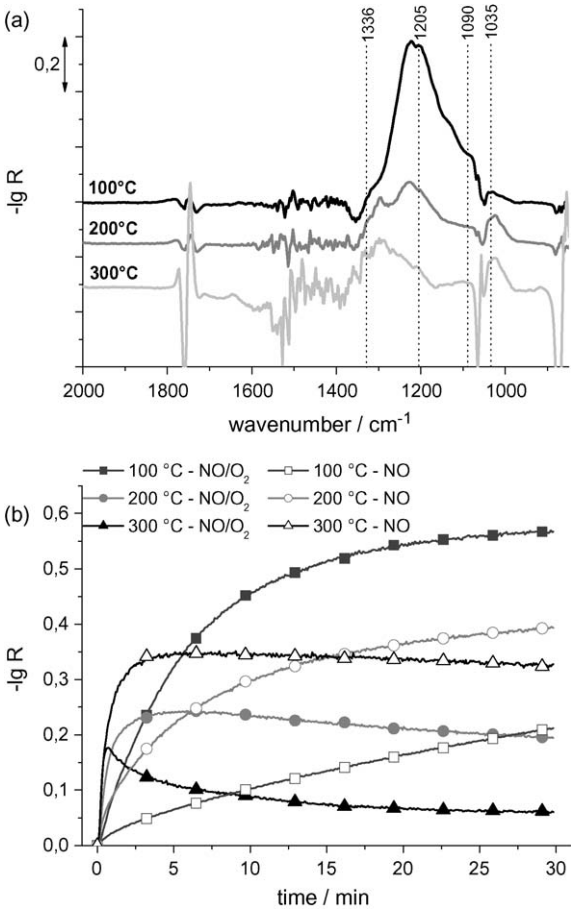

Fig. 9. (a) Temperature dependence of NO/O_2 storage on $Pt/BaCO_3$ after 30 min. (b) Development of the nitrite band at 1205 cm^{-1} during NO/O_2 and NO storage on $Pt/BaCO_3$.

3.5. NSC and the influence of NO/O_2–NO_2 equilibrium

The NO_x storage capacity of $BaCO_3$ and $Pt/BaCO_3$ was obtained by the evaluation of breakthrough curves, measured using a tubular reactor. NO_x saturation of the catalyst was assumed when the NO_x outlet concentration was equal to the NO_x inlet concentration. Due to the signal to noise ratio of the used analyser, very slow NO_x storage rates led probably to an underestimation of the NSC values, however, for technical applications these slow storage rates are anyhow not interesting. The time needed for NO_x saturation depends on the kinetic and is a function of temperature, feed composition and the chemical composition of the sample. Table 1 shows higher NSC with increasing temperature (here: 100 °C compared to 400 °C). The NSC for treatment with NO_2 is higher than for NO/O_2 which in turn is higher than for pure NO. The influence of Pt during NO/O_2 treatment especially for higher temperatures enhanced the NSC according to the DRIFTS investigations (cf. Figs. 6 and 8).

Table 1
The NO_x storage capacity of flame-made $BaCO_3$ and $Pt/BaCO_3$ in 10^{-5} mol_{NO_x} g_{cat}^{-1} (A) and the ratio of the maximal possible storage amount calculated for $BaCO_3$ (B).

Feed	100 °C $BaCO_3$		100 °C $Pt/BaCO_3$		400 °C $BaCO_3$		400 °C $Pt/BaCO_3$	
	A	B	A	B	A	B	A	B
NO	≪1	<0.1%	≪1	<0.1%	1	0.1%	1	0.1%
NO/O_2	1	0.1%	2	0.2%	4	0.4%	53	5.2%
NO_2	19	1.9%	20	2%	35	3.5%	93	9.2%

The NO_x adsorption on NSR catalyst compounds such as $BaCO_3$ is an activated process so temperatures above ca. 100 °C are necessary to store NO_x in a reasonable time. This is shown by the temperature dependence of the NO_x storage rate. Therefore, the NSC should increase with temperature as long as no NO_x desorption occurs by nitrite or nitrate decomposition. Especially for Pt-containing $BaCO_3$, the parallel temperature-depending equilibrium reaction

$$2NO_2 \rightleftarrows 2NO + O_2 \quad (2)$$

has to be considered. The equilibrium shifts to the right-hand side of Eq. (2) for higher temperatures [35] and the changed NO/NO_2 ratio with increasing NO concentration reduces the NSC as seen in Table 1 (compare feed variation experiments).

The influence of temperature was investigated by an experiment, shown in Fig. 10. $Pt/BaCO_3$ was treated with NO_2 for a certain time period. However, the sample was still far away from the maximum NSC. Starting from this condition the temperature was varied. During this experiment a constant NO_2 feed was used and the gas composition at the reactor outlet was monitored. At 200 °C the feed remained in the form of NO_2 (conversion rate to NO is only 3.5%) but the thermal activation was too low for fast NO_x storage. The conversion to NO increased to 26% after heating to 300 °C. At this temperature the thermal activation was high enough to facilitate fast NO_x storage and the NO_x breakthrough curve dropped down. This effect was reversible. Heating up to 400 °C led to a strong increase of the NO_x in the outlet and therefore less NO_x was stored. The low storage rate is attributed to the high NO_2 conversion to NO which is approx. at 75%. Very small temperature changes around 400 °C affected the NO_2 conversion remarkably which could easily rise up to 90%. An additional effect confirming the lower NO_x storage capacity is the slight thermal decomposition of stored nitrates starting at temperatures above 300 °C. Subsequent cooling down to 300 °C led again to more efficient NO_x storage.

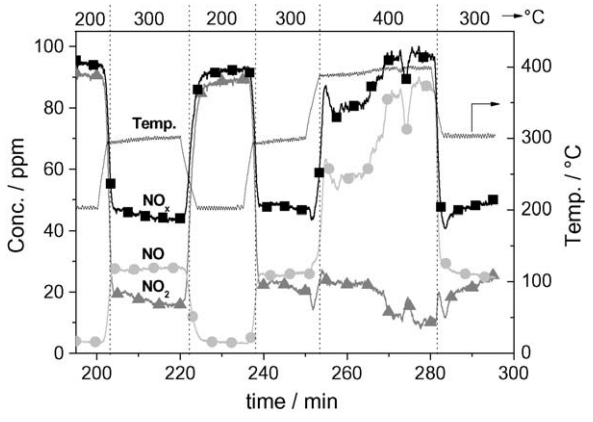

Fig. 10. Outlet gas composition during NO_2 storage on $Pt/BaCO_3$ at different temperatures.

The results indicate the benefit of a careful control of the adsorption temperature for optimal working conditions (e.g. for technical application as NSR catalyst).

3.6. Adsorption versus solid state conversion

To form $Ba(NO_3)_2$ from $BaCO_3$, NO_2 and O_2 are required according to the overall reaction [36]:

$$BaCO_3 + 2NO_2 + 0.5O_2 \rightarrow Ba(NO_3)_2 + CO_2 \quad (3)$$

or $Ba(NO_3)_2$ forms according to the modified Eq. (1), where NO and CO_2 gases are released.

$$BaCO_3 + 3NO_2 \rightarrow Ba(NO_3)_2 + CO_2 + NO \quad (4)$$

To investigate the sample with regard to barium nitrate formation, $Pt/BaCO_3$ was treated with NO_2 during a short (approx. 60 min) and a long run (approx. 20 h - until the NOx inlet and outlet were equal) at 400 °C. Ex situ DRIFT spectra from these two experiments are presented in Fig. 11a. The solid state spectrum after 60 min of NO_2 treatment indicates only a marginal change compared to the spectrum of fresh $Pt/BaCO_3$. The difference between these two spectra is shown in Fig. 11b (bottom) where bands of adsorbed nitrates can be observed (cf. Fig. 8). XRD patterns of this sample confirm that nearly the whole NO_2-treated sample remained as $BaCO_3$. Thus, formation of a significant amount of bulk nitrates could not be formed in the time period chosen.

In contrast, the DRIFT solid state spectrum of $Pt/BaCO_3$ after 20 h of NO_2 treatment shows more similarities to the spectrum of pure $Ba(NO_3)_2$ (Fig. 11a). However, this solid state spectrum does not equal neither the spectra of pure $Ba(NO_3)_2$ nor $Pt/BaCO_3$. The resulting difference after 20 h NO_2 treatment can be seen in Fig. 11b (top). When comparing these two difference spectra in Fig. 11b, a different band structure becomes apparent in the spectrum obtained after longer NO_2 treatment. This new band structure is probably caused by conversion of a part of bulk $BaCO_3$ [37] into $Ba(NO_3)_2$. The XRD pattern of this sample (see Fig. 11c) confirms the assumption of two phases. In addition to the orthorhombic $BaCO_3$ phase [31], a cubic $Ba(NO_3)_2$ phase [38] was formed. In spite of the relatively long storage time (20 h), conversion was not complete (the obtained sample consists of 55 vol.% of carbonate and 45 vol.% of nitrate according to the Rietveld method [26,27]). Thus the chosen reaction time was too short for a complete carbonate conversion although the NO_x inlet and outlet were equal and therefore saturation was assumed. As a consequence of the increasing molar volume of a storage particle during $Ba(NO_3)_2$ formation, small pores may cause a hindered diffusion into the core of the particle [36]. This effect may result in a decreased storage rate with increasing time of NO_2 treatment. At high temperatures NO/O_2 treatment of $Pt/BaCO_3$ led to the same nitrate phase but resulted in a different carbonate/nitrate ratio.

To sum up, after short NO/O_2 or even NO_2 treatment (up to 60 min) the orthorhombic $BaCO_3$ phase (XRD) remained whereas DRIFT spectra clearly showed adsorbate bands. Only long NO_x treatment at high temperatures lead to a reorganisation of the solid state lattice and consequently to the formation of bulk nitrates.

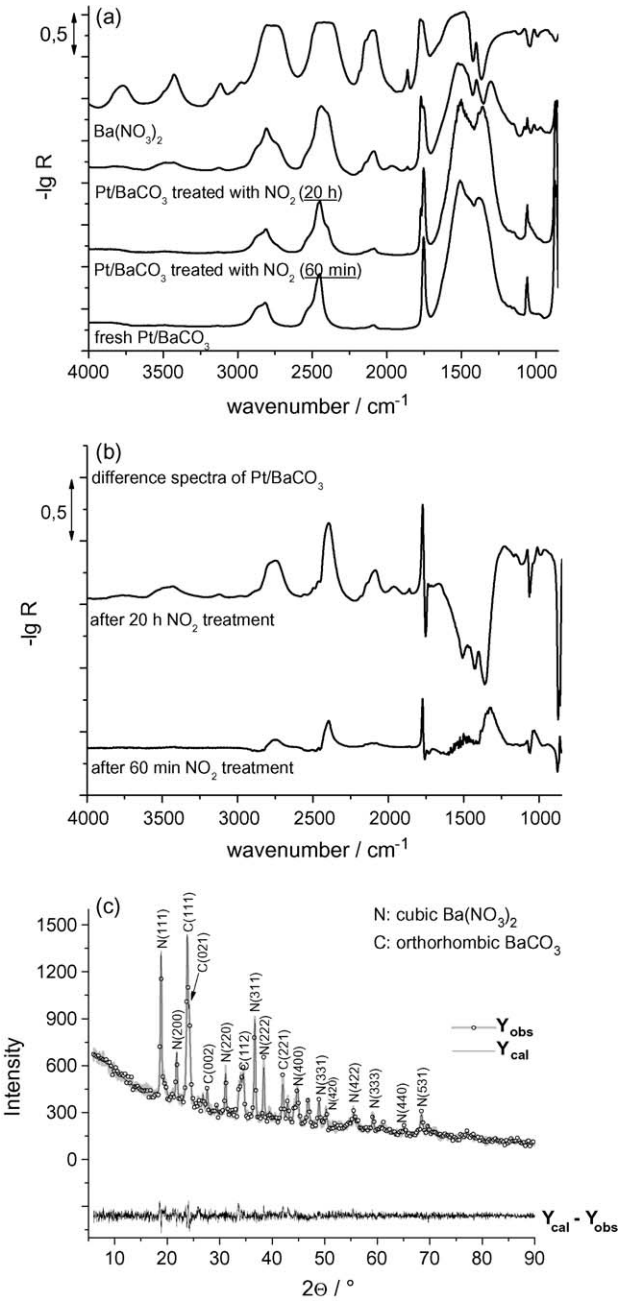

Fig. 11. (a) Solid state DRIFT spectra of $Ba(NO_3)_2$, $Pt/BaCO_3$ treated with NO_2 for 20 h and for 1 h and fresh $Pt/BaCO_3$ at 400 °C (top to down). (b) Difference in solid state spectra of fresh $Pt/BaCO_3$ with NO_2-treated $Pt/BaCO_3$ (top: after 20 h, bottom: after 60 min). (c) XRD pattern of $Pt/BaCO_3$ treated with NO_2 (20 h) with the according Rietveld analysis. Important hkl lines of $Ba(NO_3)_2$ (abbr. N) and $BaCO_3$ (abbr. C) are signed.

This means that for technical application (e.g. as NSR-automotive catalysts) NO_x adsorption on the surface and subsurface region is contributing mainly to the storage effect.

4. Conclusions

Storage of NO_x on flame-made high SSA $BaCO_3$ and $Pt/BaCO_3$ nanoparticles was studied by DRIFT spectroscopy. Adsorption of NO on $BaCO_3$ resulted in nitrites while commercially available low SSA $BaCO_3$ did not give rise to detectable bands. In contrast, NO_2 storage investigations on commercial and flame-made $BaCO_3$ showed the same adsorbed species though the latter showed more intensive bands. The presence of oxygen did not measurably affect adsorption on these Pt-free $BaCO_3$. NO_2 was stored best affording the highest NSC. DRIFT spectra suggest that during NO_2 treatment of $BaCO_3$ small amounts of NO were formed in situ, adsorbed on the surface and subsequently oxidised by excess NO_2. Higher temperatures favoured the NO_x storage process.

Addition of Pt to $BaCO_3$ changed the structure of the $BaCO_3$ and resulted in a SSA of 110 $m^2\,g^{-1}$ for the fresh powder. This SSA decreased to 60 $m^2\,g^{-1}$ after pre-conditioning of the powder at 400 °C. The Pt enhanced the NO_x storage at higher temperatures. In the presence of oxygen during NO adsorption, Pt catalysed NO oxidation and thus afforded higher NSC by direct NO_2 storage. Subsequent oxidation of previously stored NO could be corroborated by DRIFTS. The same adducts were observed upon NO_2 treatment. The maximum NSC on $Pt/BaCO_3$ was about 1 $mol_{NO_x}\,m\,g_{cat}^{-1}$ after more than 20 h of NO_2 treatment.

Considering the temperature dependent equilibrium of NO_2 and NO/O_2 as well as the need of thermal activation of NO_x storage, an optimal storage temperature exists which warrants reasonably fast storage rate coupled with high NSC. This temperature is between 300 and 400 °C for $Pt/BaCO_3$.

A few minutes of NO_x treatment afforded predominantly NO_x adsorbates on the surface. Significant bulk barium nitrate formation was only observed after long NO_x treatment at high temperatures as could be observed on $Pt/BaCO_3$. In the latter case the storage rate decreased most likely because of hindered diffusion.

The flame-made barium-containing nanopowders showed some potential for application in NSR catalysis. Due to their high surface area compared to the corresponding conventionally prepared powders, the NSC is increased, and the practical application of such nanopowders in washcoats of monoliths seems feasible.

Acknowledgements

Umicore AG & Co. KG for financial and technical support, Dipl.-Ing. Christian Schmitt for recording XRD and Dipl.-Ing. Kerstin Lehnert for BET measurements. Dr. Krumeich for TEM images and the Electron Microscopy Center of ETH Zurich (EMEZ) for providing the necessary infrastructure. Financial support ETH Research Grant TH-09 06-2 (R. Büchel) is gratefully acknowledged. The contribution of platinum chemicals by Johnson Matthey PLC is greatly appreciated.

References

[1] J. Sellman, J.D. Hamilton, Minn. Med. 90 (2007) 47–50.
[2] IPCC—Fourth Assessment Report (AR4), 2007.
[3] S. Motohisa, S. Tadashi, M. Naoto, I. Satachi, K. Kaichi, T. Toshiaki, T. Syuji, EP0613714, (1994).
[4] Z.M. Liu, S.I. Woo, Catal. Rev.—Sci. Eng. 48 (2006) 43–89.
[5] M.O. Symalla, A. Drochner, H. Vogel, S. Philipp, U. Göbel, W. Müller, Top. Catal. (2007) 199–202.
[6] W. Hauptmann, A. Drochner, H. Vogel, M. Votsmeier, J. Gieshoff, Top. Catal. (2007) 157–160.
[7] H. Grönbeck, P. Broquist, I. Panas, Surf. Sci. 600 (2006) 403–408.
[8] P.J. Schmitz, R.J. Baird, J. Phys. Chem. B 106 (2002) 4172–4180.
[9] P. Broqvist, H. Gronbeck, E. Fridell, I. Panas, Catal. Today 96 (2004) 71–78.
[10] C. Hess, J.H. Lunsford, J. Phys. Chem. B 107 (2003) 1982–1987.
[11] C. Sedlmair, K. Seshan, A. Jentys, J.A. Lercher, J. Catal. 214 (2003) 308–316.
[12] I. Nova, L. Castoldi, L. Lietti, E. Tronconi, P. Forzatti, Top. Catal. 42–43 (2007) 21–25.
[13] B. Westerberg, E. Fridell, J. Mol. Catal. A: Chem. 165 (2001) 249–263.
[14] P. Broquist, I. Panas, H. Grönbeck, J. Phys. Chem. B 109 (2005) 9613–9621.
[15] M. Piacentini, R. Strobel, M. Maciejewski, S.E. Pratsinis, A. Baiker, J. Catal. 243 (2006) 43–56.
[16] S. Balcon, C. Potvin, L. Salin, J.F. Tempere, G. Djega-Mariadassou, Catal. Lett. 60 (1999) 39–43.
[17] L. Lietti, P. Forzatti, I. Nova, E. Tronconi, J. Catal. 204 (2001) 175–191.
[18] A. Lindholm, N.W. Currier, J. Li, A. Yezerets, L. Olsson, J. Catal. 258 (2008) 273–288.

[19] F. Rodrigues, L. Juste, C. Potvin, J.F. Tempere, G. Blanchard, G. Djega-Mariadassou, Catal. Lett. 72 (2001) 59–64.
[20] A. Amberntsson, H. Persson, P. Engstrom, B. Kasemo, Appl. Catal. B 31 (2001) 27–38.
[21] M. Piacentini, M. Maciejewski, A. Baiker, Appl. Catal. B: Environ. 60 (2005) 265–275.
[22] M. Piacentini, M. Maciejewski, A. Baiker, Appl. Catal. B: Environ. 72 (2007) 105–117.
[23] R. Strobel, L. Madler, M. Piacentini, M. Maciejewski, A. Baiker, S.E. Pratsinis, Chem. Mater. 18 (2006) 2532–2537.
[24] L. Madler, W.J. Stark, S.E. Pratsinis, J. Mater. Res. 17 (2002) 1356–1362.
[25] A. Drochner, M. Fehlings, K. Krauß, H. Vogel, Chem. Eng. Technol. 23 (2000) 319–322.
[26] L.B. McCusker, R.B. von Dreele, D.E. Cox, D. Louër, P. Scardi, J. Appl. Crystallogr. 32 (1999) 36–50.
[27] T. Roisnel, J. Rodriguez-Carvajal, Mater. Sci. Forum 387–381 (2001) 118–123.
[28] R. Strobel, M. Maciejewski, S.E. Pratsinis, A. Baiker, Thermochim. Acta 445 (2006) 23–26.
[29] N.L. Wu, S.Y. Wang, I.A. Rusakova, Science 285 (1999) 1375–1377.
[30] T.S.T. Nishino, N. Ishizawa, N. Mizutani, M. Kato, J. Solid State Chem. (1987) 24–29.
[31] J.P.R. de Villiers, Am. Miner. 56 (1971) 758–766.
[32] J. Szanyi, J.H. Kwak, J. Hanson, C. Wang, T. Szailer, C.H.F. Peden, J. Phys. Chem. B (2005) 7339–7344.
[33] F. Frola, F. Prinetto, G. Ghiotti, L. Castaldi, I. Nova, L. Lietti, P. Forzatti, Catal. Today 126 (2007) 81–89.
[34] L. Olsson, E. Fridell, J. Catal. 210 (2002) 340–353.
[35] J. Després, M. Elsener, M. Koebel, O. Kröcher, B. Schnyder, W. Wokaun, Appl. Catal. B: Environ. 50 (2004) 73–82.
[36] U. Tuttlies, V. Schmeisser, G. Eigenberger, Chem. Eng. Sci. 59 (2004) 4731–4738.
[37] B. Ostrick, PhD Thesis, Justus-Liebig Universität Giessen. (2000).
[38] R. Birnstock, Z. Kristallogr. 124 (1967) 310–334.